Comparison of numerical models for the interaction of a fluid transient with an off-line air pocket

Jane Alexander[1], Zhao Li[2], Pedro J. Lee[3], Mark Davidson[4], and Huan-Feng Duan[5]

[1]Ph.D. Student, Department of Civil and Natural Resources Engineering, College of Engineering, University of Canterbury, Private Bag 4800, Christchurch 8020, New Zealand. Email: jane.alexander@pg.canterbury.ac.nz

[2]Lecturer, Department of Civil and Natural Resources Engineering, College of Engineering, University of Canterbury, Christchurch 8020, New Zealand.

[3]Professor, Department of Civil and Natural Resources Engineering, College of Engineering, University of Canterbury, Christchurch 8020, New Zealand.

[4]Professor, Department of Civil and Natural Resources Engineering, College of Engineering, University of Canterbury, Christchurch 8020, New Zealand.

[5]Associate Professor, Department of Civil and Environmental Engineering, The Hong Kong Polytechnic University, Hung Hom, Kowloon, Hong Kong.

ABSTRACT

Effective modelling of pipe network anomalies can supplement fluid transient diagnostic techniques. This study focuses on comparing modelling approaches for predicting the transient response due to air pocket entrapped outside the main flow path (off-line), in particular testing the assumption that the flow inside the cavity can be predicted based on a lumped element. This assumption has been consistently made in previous modelling investigations in the time and frequency domains. The results are compared to a system frequency response model without the lumped inertia assumption by quantifying timing and signal frequency distribution errors. It is found that removing the lumped inertia assumption improved the prediction of the reflected and transmitted pulse frequency distributions by averages of 50% and 30-35%, respectively.

INTRODUCTION

Fluid transients are an emerging technology for detecting and characterising faults in water supply networks. Common faults such as leaks, discrete blockages, extended blockages, and air pockets may identified by comparing the measured system response to the expected response given normal system conditions (Stephens et al. 2004a; Duan 2017; Duan et al. 2017; Xu and Karney 2017; Al-Tofan et al. 2019; Al-Tofan et al. 2020). As a result, it is important to understand and be able to model how different anomalies may distort transient signals in the time and frequency domains, as it may be necessary to build numerical network models to explain the expected transient response. For example, entrapped air pockets may not obstruct the flow, but even small collections can create significant transient reflections and frequency dependent effects which distort the expected response (Alexander et al. 2020b). Air tends to collect at high points in the system, including the cavities under valves and hydrants. This configuration is referred to in this paper as off-line air, as opposed to air which blocks the main flow path (in-line). The ability to accurately model off-line air may be used to improve the flexibility of transient-based diagnostic techniques.

A range of field, experimental, and numerical investigations have focused on the interaction of transients with air pockets, as air pockets may exist in pipelines either unintentionally or by design. Off-line air chambers are often installed on networks to absorb the pressures created by destructive transient events. Pockets of entrapped air may also form in the main pipe during the filling process, as a result of biological activity, or via vortex action at air chamber entrances (Lauchlan et al. 2005). Martin and Wiggert (1986) noted that cooling systems, such as those in power stations, are prone to developing bubbles, slugs, or large masses of entrapped air, due to entry of air at the intake, through leaking seals, or as a result of gas release due to fluctuations in pressure or temperature. Many transient researchers have focused on the case of an air pocket entrapped at the end of a filling pipe, finding that smaller air pockets led to increased transient pressures due to acceleration, and large air pockets resulted in lower peak transient pressures than those observed for the no-air case due to the additional energy absorption provided (Jönsson 1985; Lee and Martin 1999; Zhou 2000; Lee 2005; Zhou et al. 2011; Vasconcelos and Leite 2012). The sudden collapse of air pockets

within pipes may also create unexpectedly large transient pressures, greater in magnitude than the Joukowsky head rise (Bergant et al. 2006).

A number of methods exist for modelling fluid transients in the time domain, including the Method of Characteristics (MOC), explicit and implicit finite difference methods, finite element techniques, and the Lagrangian wave characteristic model (Wood et al. 2005). Of these, the MOC, a finite difference method, is the most well known and widely researched, as it provides accurate results with relative computational efficiency and ease of programming (Chaudhry 1979). Pipeline anomalies, like off-line air pockets, can be incorporated as boundary conditions. Off-line air pockets, or air chambers, are most commonly incorporated into the MOC using the simple accumulator equation (Wylie et al. 1993), which uses the polytropic relationship to describe the dynamics of the air pocket. The accumulator equation has been previously used successfully as part of large-scale field investigations for the in-line pocket application (Burrows and Qiu 1995; Stephens et al. 2004b). For off-line pockets which entirely fill their cavity, with no connecting water column, experimental tests using high frequency transients found that the polytropic equation alone was able to provide an accurate prediction of the magnitude, shape and timing of the overall pressure trace (Kim 2008b). However, in many cases off-line pockets do not entirely fill their confining cavity, and are connected to the main flow by a short water column. Experimental and field investigations have noted that the dimensions of the connecting section influence the transient response, especially when it is throttled (Wylie et al. 1993; De Martino and Fontana 2012). Early studies on air chamber design used a local loss coefficient for the throttled section (Evans and Crawford 1954; Fok 1978; Purcell 1997), which was later deemed to be an unrealistic assumption and no longer justifiable due to the availability of computing power, as in reality hydraulic losses will also occur in the connecting pipeline section separating the water-air interface and the main pipe (Graze and Forrest 1974). This resulted in the development of the lumped inertia model, which accounts for friction and inertia effects in the connecting section by assuming it is incompressible and inertia in the connector dominates the transient response (Graze and Forrest 1974; Wylie et al. 1993). Zhou et al. (2013) and Zhou et al. (2018) have also noted that heat exchange can be important when

predicting energy dissipation due to the air-transient interaction. The lumped inertia assumption has not previously been tested against an MOC model without simplifying assumptions. This may be attributable to one of the key drawbacks of the MOC as a solution scheme: that its efficiency is affected by the number of nodes (Duan et al. 2018), and the discretization required to accurately model short connectors will significantly increase computational costs.

Alternatively, the system response to transient events may be modelled in the frequency domain, using transfer matrices to linearize the frequency domain equivalents of the governing 1D mass and momentum equations. Since the first studies on frequency domain analysis (Jönsson and Larson 1992), multiple studies have found that the presence of pipeline anomalies such as leaks and discrete and extended blockages affect the peaks of the frequency response (Lee et al. 2005; Lee et al. 2008; Duan et al. 2012). As a result, the system frequency response (SFR) approach has become more popular in recent years for pipeline condition assessment via inverse analysis, as short pipe defects can be efficiently incorporated into the model without increasing the computational effort (Lee et al. 2013; Duan and Lee 2016). Frequency domain modelling also allows increased flexibility over time domain modelling in that transient generators and receivers can be placed at any location, and are not limited by the MOC discretization. Although the theory for modelling off-line air pockets in the frequency domain is shown in Wylie et al. (1993), air pockets have not been incorporated into the SFR approach in the condition assessment field to date. Similar to the MOC approach in the time domain, the governing equations are based on the lumped inertia assumption, and the effect of this assumption on the model accuracy has not been evaluated.

The purpose of this study is to use experimental results to test the lumped inertia assumption for modelling the reflection and transmission of a high frequency transient past an off-line air pocket. The governing equations have not previously been validated for experiments of this nature. Three modelling approaches will be tested: the MOC with lumped inertia (MOC-LI), the SFR approach with lumped inertia (SFR-LI), and an SFR approach employing plane wave theory which does not make a lumped inertia assumption (SFR-PW). An SFR method was selected to model the air pocket without the lumped inertia assumption due to its efficiency compared to the MOC, as discussed

previously. The MOC accumulator equation for the in-line air pocket scenario has been previously used as part of large-scale field investigations (Burrows and Qiu 1995; Stephens et al. 2004b; Gong et al. 2014), while this investigation is primarily aimed at testing the applicability of the equations for the off-line pocket response. This investigation is part of a group of articles on the interaction of transients with air pockets, and follows an earlier experimental investigation comparing the effects of in-line and off-line pockets (Alexander et al. 2020b), as well as experimental and numerical investigations into the in-line air configuration (Alexander et al. 2019; Alexander et al. 2020a). The results can be incorporated into transient fault detection techniques to account for the effects of off-line air on the transient response.

EXPERIMENTAL PROCEDURE

The experimental set-up is shown in Fig. 1. It consisted of a 41.6 m straight steel pipe, of 22.25 mm internal diameter, inclined at an angle of 3.5°. The system dimensions were primarily set by space limitations within the lab. The relatively small pipe diameter was selected to ensure the transient pulse generated and subsequent reflections would be clearly visible in the measured data. A reservoir at the downstream end of the system was used to pressurize the system. At the upstream end of the pipe, a Baccara solenoid valve was used to generate the transient. The valve was programmed to open and close over a 6 ms period, generating a signal of a similar frequency range to that used in transient fault detection. Note that the nomination of the upstream and downstream boundary are in relation to the origin point of the transient, as there is no flow in the system. The solenoid pulse has an amplitude of approximately 0.4 relative to the initial hydrostatic pressure of the system, and a frequency range of approximately 0-1.5 kHz. Three PCB Piezotronics Model 102A07 dynamic pressure transducers were fitted along the system to measure the resultant pressure disturbances. The transducers have a 345 kPa measuring range, a natural frequency of over 250 kHz, and an uncertainty of 3.45 kPa. A sampling frequency of 10,000 Hz was used, and recorded the pressure response for 5 seconds following the solenoid movement. Computer control of the solenoid valve and transducers was programmed using National Instruments LabView software. The electronic trigger for the solenoid valve was abrupt, but the mechanical response of

the valve resulted in a smooth disturbance without tripping. The 6 ms cycle time was based on the computer clock, meaning the difference from the wall-clock time was within several tens of nanoseconds, and therefore negligible relative to the transient pulse length.

Part way along the pipe (Section A-A') was a steel crest section, as shown in Fig. 2. A fourth dynamic pressure transducer was fitted at the top of the crest. A steel cavity of length 177 mm (L_{cavity}) and diameter 8.5 mm (D_{cavity}) was screwed to the top of the crest. There was a short neck section between the cavity and the main pipe, which had a length of 24.9 mm (L_{neck}) and a diameter of 6.3 mm (D_{neck}). A bleed valve at top of the cavity was used to insert the air pocket, using a measuring syringe. The volume of air was measured before insertion, and the air was extracted and measured again at the end of the test to ensure no air had moved from the cavity. Nine air pocket volumes were tested, ranging from 1.25 ml to 29.4 ml at atmospheric pressure (V = 1.25, 5.0, 8.9, 12.8, 17.1, 21.0, 23.8, 25.7, and 29.4 ml), and range between 4% and 90% of the total cavity length (L_{cavity}) once pressurized. Each air pocket volume was tested at 6 initial hydrostatic pressures, ranging between 0.5 and 3 bar in 0.5 bar increments. The pocket volumes are converted to pressurized in-pipe volumes using the polytropic equation: $H_A V^n = C_A$, where H_A is the absolute head at the pocket, V the pocket volume, n the polytropic exponent, and C_A the polytropic constant which can be calculated using the initial conditions. A mid-range polytropic exponent of 1.2 was assumed in this work (Wylie et al. 1993). Transient testing was repeated 10 times for each set of experimental conditions, and the standard errors were observed to be less than 0.05% of the absolute pressure readings on average. The tests were carried out with no base flow to prevent the air being shifted by the flow, and the pipe was bled at side discharge valves along its length between each air pocket test. At the end of each test, the full volume of air was retrieved from the cavity, confirming no air dissolution or movement. Noise in the system was also observed to be minor. Before the generation of the transient, the average pressure disturbance measured at the pressure transducers was approximately 0.05% of the initial hydrostatic pressure, with the maximum deviation from zero approximately 1.4% of the initial hydrostatic pressure. No artificial noise was incorporated into the numerical models.

GOVERNING EQUATIONS

Method of Characteristics - Lumped Inertia Model

The MOC approach comprises a set of characteristic equations described in detail by Wylie et al. (1993), based on the governing mass and momentum equations for 1D unsteady pipe flow

$$\frac{\partial H}{\partial t} + \frac{a^2}{g}\frac{\partial U}{\partial x} = 0 \,, \tag{1}$$

$$\frac{\partial U}{\partial t} + g\frac{\partial H}{\partial x} + g h_f = 0 \,, \tag{2}$$

where H is the piezometric head, U the fluid mean velocity, a the pipeline wave speed, x the distance along the pipe, t the time, g the acceleration due to gravity, and h_f the friction loss per unit length. Both steady and unsteady friction were included in the MOC using the equations described in Zielke (1968). Zielke's weighting function for unsteady friction is best suited to laminar flow regimes. The experimental system is expected to satisfy this requirement given the lack of base flow. The modelling was implemented with 308 spatial nodes and the time step was set to match the experimental time step. This was compliant with the Courant stability condition. Sensitivity testing carried out for the MOC discretization showed that further increases in the number of spatial nodes used did not result in significant differences in the modelled pressure traces over the time period of interest (the first reflected and transmitted pulses). For instance, increasing the spatial discretization from 308 nodes to 1000 nodes resulted in an average variation of 0.004% in the modelled pressures.

The off-line air chamber was incorporated into the MOC as a boundary condition. It was assumed the air within the cavity behaves according to the polytropic relationship defined previously ($H_A V^n = C_A$). This can be written at the end of the time interval Δt as

$$(H_P + \bar{H} - z)(V + \Delta V)^n = C_A \,, \tag{3}$$

where H_P is the gauge pressure at the pocket, $\bar{H}$ the atmospheric pressure, z the elevation of the pipe above the datum, V the pocket volume at the beginning of the time interval, ΔV the volume change across the time interval, and n the polytropic exponent. In the lumped inertia model, at a given time index j the head at the air-water interface is linked to the head at the junction with the main pipe according to the following:

$$H_j^J - H_j^S = C_{c1} + C_{c2} Q_j^{ext} \tag{4}$$

$$C_{c1} = H_{j-1}^S - H_{j-1}^J - \left(\frac{8L_c}{g\pi D_c^2 \Delta t} + \frac{8L_n}{g\pi D_n^2 \Delta t} \right) Q_{j-1}^{ext} \tag{5}$$

$$C_{c2} = \left(\frac{8L_c}{g\pi D_c^2 \Delta t} + \frac{8L_n}{g\pi D_n^2 \Delta t} \right) + \left(\frac{16 f_n L_n}{g\pi^2 D_c^5} + \frac{16 f_n L_n}{g\pi^2 D_n^5} \right) |Q_{j-1}^{ext}| \tag{6}$$

where H^J is the head at the junction, H^S the head at the water surface, Q^{ext} the flow into the off-line section, L_c and L_n the length of the cavity and neck sections, D_c and D_n the diameter of the cavity and neck sections, and f_c and f_n the Darcy-Weisbach friction factors for the flow in the cavity and neck sections, using the formulation for laminar flow based on the flow velocity in the connection at the previous time step. Sensitivity testing was carried out to compare possible formulations for friction. Three cases were tested for the flow regime in the connector: laminar for all time, turbulent for all time, and turbulent or laminar based on the velocity in the previous time step. The average variation between the three cases was approximately 0.08% during the first three periods. The flow was assumed to be laminar for all time for consistency with the SFR-LI, as only one regime can be set for this case. The inclusion of laminar or turbulent unsteady friction in the connector was also tested using the SFR-LI (Vítkovskỳ et al. 2003), with the average variation approximately 0.17% in the first three periods compared to steady friction alone. Unsteady friction in the connector was therefore not considered in this work, in accordance with the equations presented in the literature (Karney and McInnis 1992; Kim 2008a). The key physical quantities and locations are shown in Fig. 3. These can be combined with the MOC equations and solved for Q_j^{ext}. The governing equations of the lumped inertia model are outlined in further detail by Karney and McInnis (1992) and Kim (2008a), and the full derivation can be found in Wylie et al. (1993).

Zhou et al. (2013) and Zhou et al. (2018) have noted in previous studies that heat transfer effects may be important when modelling the transient energy dissipation, with 3D computation fluid dynamics (CFD) modelling used describe dissipation in their simulation. Zhou et al. (2013) states that the temperature change is related to the volume change of the pocket, with pocket compression leading to increased temperatures within the air. Zhou et al. (2013) and Zhou et al. (2018) observed that their experimental system became noticeably hot to the touch, and although lag associated with the temperature transducer meant that the actual temperature changes could not be accurately recorded, 3D modelling with heat transfer considerations was able to more accurately predict the long-term pressure response. It is expected that heat exchange effects will be less influential for this application, given the relatively small size of the transient pulses generated ($\Delta H \approx 0.2 - 1.2$m) compared to Zhou et al. (2013) and Zhou et al. (2018) ($\Delta H \approx 20 - 35$ m). Furthermore, the primary aim of this paper is to evaluate the model prediction for the first reflected and transmitted pulses. Testing from Zhou et al. (2018) showed that even though the 3D model predicted significant temperature increases within the air, the outputs only began to diverge from 1D models for later reflections as the discrepancies in the predicted energy losses began to accumulate. For these reasons, temperature variations and heat transfer between the air and adjacent water during the transient process were not considered as part of the MOC or in the SFR modelling described in the following subsections.

System Frequency Response: Lumped Inertia Model

In the frequency domain, concatenated transfer matrices are used to represent adjacent pipeline elements. The transfer matrix is a linearized frequency domain version of the governing mass and momentum equations for 1D flow (Eqs. 1 and 2). For the experimental pipe system consisting of pipe elements connected in series, the general form of the transfer matrix equation is (Chaudhry 1979)

$$\begin{Bmatrix} q \\ h \\ 1 \end{Bmatrix}^1 = \boldsymbol{P_0 A_0 P_1 G_0} \begin{Bmatrix} q \\ h \\ 1 \end{Bmatrix}^0 \tag{7}$$

$\boldsymbol{P_0}$, $\boldsymbol{A_0}$, $\boldsymbol{P_1}$, and $\boldsymbol{G_0}$ are the transfer matrices for the pipe section between the downstream tank and the off-line pocket, the off-line pocket section, the pipe section between the off-line pocket and the solenoid, and the solenoid transient generator, respectively. These link the perturbations in head h and discharge q at the closed upstream valve (superscript 0), to those at the downstream boundary (superscript 1). The extended 3×1 form is used to account for elements with external forcing.

The transfer matrix for the intact pipe section is given by (Wylie et al. 1993)

$$\boldsymbol{P_n} = \begin{bmatrix} \cosh(\mu L) & -\frac{1}{Z_c}\sinh(\mu L) & 0 \\ -Z_c \sinh(\mu L) & \cosh(\mu L) & 0 \\ 0 & 0 & 1 \end{bmatrix} \tag{8}$$

where L = pipe section length; $\mu = (\omega/a)\sqrt{1 - igAR/\omega}$; $Z_c = \mu a^2/i\omega g A$; ω = frequency; and i = imaginary unit. The subscript n used in Eqs. 8-10 refers to the index of the pipe element for which the transfer matrix is calculated. The friction term R is the summation of steady (R_S) and unsteady (R_U) terms. The steady friction term $R_S = fQ/gDA^2$, where f = friction factor; D = pipe diameter; and A = pipe cross-sectional area. The experimental system has zero base flow and therefore exists in the laminar flow region, so the unsteady term was calculated using the integral solutions for Zielke's weighting function in the frequency domain, provided by Vítkovskỳ et al. (2003).

For the system frequency response with lumped inertia (SFR-LI), the off-line cavity represents a junction with the extended transfer matrix (Wylie et al. 1993)

$$\boldsymbol{A_n} = \begin{bmatrix} 1 & \frac{1}{Z_A} & 0 \\ 0 & 1 & 0 \\ 0 & 0 & 1 \end{bmatrix} \tag{9}$$

where Z_A is the impedance of the off-line cavity adjacent to the main pipe. Using the lumped inertia assumption, the impedance of an air chamber is given by $Z_a = in\bar{H}_A/\forall\omega$, where $\bar{H}_A$ is the absolute head at the pocket. This can be adjusted to the impedance at the base of the connector

adjacent to the main pipe, $Z_A = Z_a - (R_c + i\omega/gA_c)l_c - (R_n + i\omega/gA_n)l_n$, where R_c and R_n are the resistances associated with the cavity and neck, A_c and A_n are the cross-sectional areas of the cavity and neck, and l_c and l_n are the lengths of the cavity and neck.The resistance term is defined as $R = 32\nu/gAD^2$, where D is the diameter of the cavity or neck (Wylie et al. 1993).

For a unit perturbation, the transfer matrix for the transient generator is given by

$$\boldsymbol{G_n} = \begin{bmatrix} 1 & 0 & 1 \\ 0 & 1 & 0 \\ 0 & 0 & 1 \end{bmatrix} \tag{10}$$

Multiplying the field matrices for each element results in a 3×3 universal matrix describing the system, U. Expanding Eq. 7 therefore gives

$$q^1 = U_{11}q^0 + U_{12}h^0 + U_{13} \tag{11}$$

$$h^1 = U_{21}q^0 + U_{22}h^0 + U_{23} \tag{12}$$

where U_{ij} are the system matrix elements. For the experimental system, the boundary conditions are $q^0 = h^1 = 0$, meaning the head response at the closed valve is given by $h^0 = -U_{23}/U_{22}$. Once h^0 is known it can be used to calculate the system response, h^1, at any receiver in the system using Eq. 12 and the relevant transfer matrix U based on the pipe elements between the closed valve and the receiver. The actual response is obtained by multiplying h^1 by the spectra of the input pressure disturbance of the solenoid. The input spectra is the Fourier transform of the time domain head disturbance.

System Frequency Response: Plane Wave Model

The same approach as defined in the previous section for the system frequency response is used in the SFR-PW model. However, the plane wave assumption is used to derive the transfer matrix for the off-line air pocket section ($\mathbf{A_0}$). This derivation assumes that the cavity and neck section of the off-line section are compressible without the simplification of lumped inertia. The plane wave

is a case which applies when physical quantities, in this case pressure and velocity, are constant across the plane perpendicular to the direction of movement (Kinsler et al. 2000). The assumption was used here as the pressure and velocity variation across the cross-section is small compared to the longitudinal variation along the pipe length. A schematic of the offline pocket system is shown in Fig. 4. The off-line air pocket system is composed of a main pipeline, a neck connecting to the cavity, a cavity filled with water, and an air pocket entrapped at the top of the cavity. These four regions are denoted with superscripts p, c, a, and n to distinguish physical parameters in different regions. The subscripts in, rf, and tr represent incident, reflected, and transmitted waves.

At the four boundaries in the system, head (H) and flow (Q) must satisfy continuity boundary conditions. Assuming that the waves considered have a wavelength much larger than the neck diameter, the boundary conditions are given below.

Boundary 1:

$$H^p_{in} + H^p_{rf} = H^p_{tr} = H^n_{tr} + H^n_{rf} \tag{13}$$

$$Q^p_{in} - Q^p_{rf} = Q^p_{tr} + Q^n_{tr} - Q^n_{rf} \tag{14}$$

Boundary 2:

$$H^n_{tr} + H^n_{rf} = H^c_{tr} + H^c_{rf} \tag{15}$$

$$Q^n_{tr} - Q^n_{rf} = Q^c_{tr} - Q^c_{rf} \tag{16}$$

Boundary 3:

$$H^c_{tr} + H^c_{rf} = H^a_{tr} + H^a_{rf} \tag{17}$$

$$Q^c_{tr} - Q^c_{rf} = Q^a_{tr} - Q^a_{rf} \tag{18}$$

Boundary 4:

$$Q^a_{tr} = Q^a_{rf} \tag{19}$$

If the amplitude of the incident wave (H^p_{in}) is normalized to 1, under the plane wave assumption the amplitude of the reflected and transmitted waves correspond to reflection and transmission coefficients (denoted as R and T) in each region. Considering the relationship $Q = HA/\rho a$, where a = wave speed in each region, A = cross-sectional area of each region, and the pipeline impedance $Z = \rho a/A$ in each region, Eqs. 13-19 can be rewritten as

$$1 + R^p_{rf} = T^p_{tr} = T^n_{tr} + R^n_{rf} e^{ik^n L^n} \tag{20}$$

$$\frac{1}{Z^p}(1 - R^p_{rf}) = \frac{1}{Z^p} T^p_{tr} + \frac{1}{Z^n}(T^n_{tr} - R^n_{rf} e^{ik^n L^n}) \tag{21}$$

$$T^n_{tr} e^{ik^n L^n} + R^n_{rf} = T^c_{tr} + R^c_{rf} e^{ik^c L^c} \tag{22}$$

$$\frac{1}{Z^n}(T^n_{tr} e^{ik^n L^n} - R^n_{rf}) = \frac{1}{Z^c}(T^c_{tr} - R^c_{rf} e^{ik^c L^c}) \tag{23}$$

$$T^c_{tr} e^{ik^c L^c} + R^c_{rf} = T^a_{tr} + R^a_{rf} e^{ik^a L^a} \tag{24}$$

$$\frac{1}{Z^c}(T^c_{tr} e^{ik^c L^c} - R^c_{rf}) = \frac{1}{Z^a}(T^a_{tr} - R^a_{rf} e^{ik^a L^a}) \tag{25}$$

$$\frac{1}{Z^a} T^a_{tr} = \frac{1}{Z^a} R^a_{rf} e^{ik^a L^a} \tag{26}$$

where L = region length and $k = \omega/a$. The off-line pocket system behaves as a two-port network, with the reflection and transmission coefficients forming a scattering matrix (Orfanidis 2002)

$$S = \begin{bmatrix} S_{11} & S_{12} \\ S_{21} & S_{22} \end{bmatrix} = \begin{bmatrix} R^p_{rf} & T^p_{tr} \\ T^p_{tr} & R^p_{rf} \end{bmatrix} \tag{27}$$

This can be converted to a transfer matrix T for the off-line pocket system with the following elements (Martin 2015)

$$T_{11} = \frac{(1 - S_{11})(1 + S_{22}) + S_{12}S_{21}}{2S_{21}} \tag{28}$$

$$T_{12} = \frac{(1 - S_{11})(1 - S_{22}) - S_{12}S_{21}}{2S_{21}} \tag{29}$$

$$T_{21} = \frac{(1 + S_{11})(1 + S_{22}) - S_{12}S_{21}}{2S_{21}} \tag{30}$$

$$T_{22} = \frac{(1 + S_{11})(1 - S_{22}) + S_{12}S_{21}}{2S_{21}} \tag{31}$$

The extended form of the transfer matrix for the off-line air pocket is therefore

$$\boldsymbol{A_n} = \begin{bmatrix} T_{11} & T_{12} & 0 \\ T_{21} & T_{22} & 0 \\ 0 & 0 & 1 \end{bmatrix} \tag{32}$$

The frequency domain modelling approach analyzes the response at one frequency at a time. It should be noted that this is not a representation of the valve operation in reality. Taking into account the spectrum of the pulse signal, allows the model output to be converted back into the time domain. The work in this paper is not related to the frequency-based condition assessment work presented in the literature.

RESULTS

Model Outputs

The outputs of the three models (MOC-LI, SFR-LI, SFR-PW) are plotted in the time domain to show the performance of the models in predicting the first reflected and transmitted pulses from the off-line air pocket. Figures 5 and 6 compare the modelled and measured pressure traces on either side of the air pocket for three representative pocket volumes. Time t was normalized by the pipeline period ($t^* = \frac{a}{4L}t$), while the pressure disturbance H was normalized by the initial hydrostatic pressure H_0 ($H^* = \frac{H}{H_0}$). The pressurized volume of the off-line air pocket was converted to a length ($L_a = \frac{\forall}{A_{cavity}}$) and normalized by the length of the cavity ($L_a^* = \frac{L_a}{L_{cavity}}$). The first pulses

297 reflected and transmitted by the air pocket are boxed in Figs. 5 and 6, respectively. All three models
298 were able to predict the general shape of the first reflected and transmitted pulses, capturing the
299 pressure peaks and following low pressure tails, with some discrepancy in the amplitude, shape,
300 and timing of the pressure disturbances. As the transient progressed, the differences between
301 the three models were compounded by further air pocket reflections and transmissions, boundary
302 reflections, and hydraulic and thermal energy losses in the system. A cursory inspection of the
303 pressure traces suggested that the frequency domain models (SFR-LI, SFR-PW) provided the most
304 accurate prediction of the upstream response at PT2 in terms of the wave shape and timing, while
305 the time domain model (MOC-LI) provided a more accurate prediction of the downstream response
306 at PT3. A detailed investigation of the model performance was required to assess the accuracy of
307 the lumped inertia approach for modelling the off-line air pocket scenario.

308 **Assessment Approach**

309 The following sub-sections evaluate the accuracy of the three models (MOC-LI, SFR-LI, SFR-
310 PW) in predicting the transient response. Key measures of the model fit are identified and used to
311 quantify the accuracy for the range of experimental scenarios considered.

312 The primary purpose of this investigation was to assess methods for predicting the off-line air
313 pocket response, which can be incorporated into larger system models in the future. To this end, the
314 model performance assessment centred on the first pulses reflected and transmitted by the off-line
315 air pocket. Subsequent pressure disturbances are also influenced by system boundary reflections
316 and network losses, which are not the focus of this investigation. Example pulses are boxed in
317 Figs. 5 and 6. It should be noted that the extended low pressure tails following both pulses were
318 interrupted by subsequent reflections. This means the entire pulse created by the air pocket cannot
319 be considered, and the pulses used for analysis were cut off at approximately the locations boxed
320 on Figs. 5 and 6. This affects the quantification of the pulse signal frequency distribution as
321 introduced later. However, the outputs of the three modelling approaches were treated in the same
322 manner, and the succeeding parts of the extended tails are of low amplitude relative to the rest of
323 the pulse and are predicted similarly by the three models. This suggests the frequency distribution

errors calculated are not significantly biased by the approach.

The primary properties of the transient response which can be used to assess model performance are timing and frequency distribution. Errors in both these properties were evident in the traces presented in Figs. 5 and 6, so the model assessment aimed to quantify and compare errors in these properties between the three modelling approaches.

Peak Arrival Time Error

Since the MOC and SFR modelling approaches are based on the same equations, the arrival time of the initial pressure disturbance created by the solenoid was identical between the three models, as can be observed in Fig. 5. The timing of the subsequent transient peaks, which are easily identifiable, may be used as a basic property for characterizing the air pocket location. The variations in pulse shape between the predictions of the three models meant that the arrival times of the reflected and transmitted peaks (marked on Figs. 5 and 6) differed between the three cases. Note that the precision level of the numerical models was set to match the experimental precision, and the spatial locations of the air pocket section and sensors were matched between the two models based on the MOC discretization. The errors in the arrival time of the peaks were quantified using the time difference between the arrival of the incident pulse peak, and the arrival of the first reflected and transmitted peaks. The error was calculated as

$$\epsilon = \frac{\Delta t_{mod} - \Delta t_{exp}}{\Delta t_{exp}} \tag{33}$$

where Δt is the time difference between the arrival of the incident peak at PT2 and the arrival of either the reflected peak at PT2 or the transmitted peak at PT3. The peak arrival time errors calculated for each experimental scenario are shown in Fig. 7. The SFR peak arrival time errors are only plotted once, as the SFR-LI and SFR-PW models resulted in similar errors. For the experimental scenarios tested, there was no significant trend in the peak arrival time error initial hydrostatic pressure for either modelling approach, and a weak negative correlation with pocket volume across the range of volumes tested. On average, the MOC approach over-predicted the

arrival time for the reflected peak by 2.6%, and under-predicted the arrival time for the transmitted peak by 0.8%. Meanwhile, the SFR approach over-predicted the arrival time for both the reflected and transmitted peaks, by an average of 3.5% and 0.4%, respectively. The timing analysis showed that the two approaches performed comparatively for the reflected and transmitted peak timing. On average, the errors were approximately 1-2 time steps.

Signal Frequency Distribution Error

The pulses reflected and transmitted by the air pocket were converted to the frequency domain to assess the signal frequency distribution. The advantage of conversion to the frequency domain is that the shape and amplitude of the pulse can be considered simultaneously, whereas they may be difficult to separate in the time domain. A discrete Fourier transform (DFT) was used to obtain the magnitude of each frequency contained in the time domain pulses. Figure 8 shows example DFTs for the reflected and transmitted pulses. The frequency ω was normalized by the inverse of the pipeline period ($\omega^* = \frac{4L}{a}\omega$), while the amplitude was normalized by the initial hydrostatic pressure ($h^* = \frac{h^*}{H_0}$).

The model performance was quantified using relative root mean squared error (RMSE) for the pulse DFTs. The RMSE is given by

$$RMSE = \sqrt{\frac{1}{n}\sum_{i=1}^{n}\left(\frac{(y_i - \hat{y}_i)^2}{y_i}\right)} \tag{34}$$

where n is the number of observations, y is the observed data series and $\hat{y}$ is the predicted data series. The RMSE was calculated for frequencies up to the point at which the signal has almost entirely damped ($h^* < 2$). Figure 9 shows the RMSEs obtained for the three models for the range of pocket sizes tested. Note that there was no significant trend in the RMSE of the normalized DFTs with initial hydrostatic pressure.

Figure 9 shows that, for the reflected pulse DFT, the RMSE for all models tended to increase with increasing air pocket size. The exception to this observation was the smallest pocket volume tested ($L_a^* \approx 0.05$), which resulted in comparably large errors, suggesting the model performance

is reduced for pocket volumes which are small relative to their confining cavity. It has been noted previously for the in-line pocket case that the time domain response for small pocket volumes differs significantly to that observed for larger volumes (Alexander et al. 2020a). This was also the case for the smallest off-line volumes tested. This was thought to be due to the fact that for small pocket volumes the transient response has a greater dependence on the instantaneous volume change, as opposed to the steady state volume (Alexander et al. 2020a). The reduced performance observed for small pocket volumes in Fig. 9 suggests that the models do not account for this effect of air volume on the air-transient dynamic. The RMSEs calculated indicate that pockets below $L_a^* \approx 0.3$ are approaching this transition point, as below this threshold the RMSE tended to increase with decreasing pocket volume, particularly for the MOC-LI model. For the range of medium to large pocket volumes tested ($L_a^* > 0.3$), the SFR-PW model generally resulted in the lowest RMSE for the reflected pulse DFT. The RMSE associated with all three models followed an approximately quadratic trend with volume. There was no significant trend in the relative magnitude of the RMSE between the three models for the range of pocket volumes tested. For the reflected pulse, the RMSE for SFR-PW model was approximately 50% of that observed for the MOC-LI and SFR-LI models on average.

Figure 9 shows that, for the transmitted pulse DFT, the RMSE for all models tended to increase with increasing air pocket size for $L_a^* \gtrsim 0.4$, from RMSE$\approx$ 0.1 to RMSE$\approx$ 0.5. Below this threshold, a larger degree of variability was evident, with errors of up to RMSE$\approx$ 0.9 observed. Inspection of the data indicated that this is partly related to errors associated with the resonance behaviour of the pocket. As noted in Alexander et al. (2020b), the transmitted pulse DFT reaches a sharp local minimum at the resonant frequency of the pocket (at $\omega^* \approx 4$ for the DFT shown in Fig. 8b). Due to the sharpness of this section of the transmitted pulse DFT, variations in the location of the local minimum visibly affect the RMSE, with a moderate correlation observed between the RMSE and the error in the modelled resonant frequency compared to the experimental observation. Greater variation in the resonant frequency error was evident for $L_a^* \lesssim 0.4$, corresponding with the variation observed in the RMSE for this range. For $L_a^* \gtrsim 0.4$, the RMSE for SFR-PW model

was approximately 68% of that observed for the MOC-LI model, and approximately 65% of that observed for the SFR-LI model on average.

For both the reflected and transmitted pulses, future modelling efforts should primarily aim to improve the prediction accuracy for small pocket lengths. This may include considerations for both the instantaneous volume changes and consistency with regards to capturing the resonant frequency. However, the general findings for the range of data collected show that consideration of the transient as a plane wave which interacts with each interface in the off-line section separately, rather than treating the section as a lumped body of fluid, is generally able to provide greater accuracy in the signal frequency distribution of the transient pulse for this experimental case.

CONCLUSIONS AND RECOMMENDATIONS

Off-line air pockets may not adversely affect the operation of pipeline systems, but may interfere with transient-based condition assessment techniques. This means it is important to understand how they may be included in network models. The major assumption in past modelling of off-line air pockets has been the lumped inertia assumption, which infers that the connecting water column between the off-line pocket and the main pipe behaves as an incompressible unit. This study tested this assumption in the method of characteristics (MOC-LI) and a system frequency response model (SFR-LI) against a system frequency response model which does not assume an incompressible unit at the connector (SFR-PW).

The outputs of the three models for the first pulses reflected and transmitted by the air pocket were compared to experimental data for a range of pocket volumes and initial hydrostatic pressures. Two properties of the first reflected and transmitted pulses were used to assess the models' performance: timing and signal frequency distribution. It was found that error in the pressure peak arrival time was primarily dependent on the modelling approach used, with the MOC model performing better than the SFR models. However, both models had average peak arrival time errors of less than 4%. As discussed previously, an MOC model for off-line air pockets which does not use the lumped inertia assumption is likely to require significant additional computing power, which may outweigh the additional benefit with regards to timing. With regards to the frequency distribution error, the

SFR-PW model resulted in an approximately 50% improvement in the prediction of the reflected pulse frequency distribution and an approximately 30-35% improvement in the prediction of the transmitted pulse frequency distribution compared to the lumped inertia models. This indicates that, for the experimental conditions tested, the lumped inertia assumption results in a reduction in the model performance with regards to the pulse frequency distribution. The differences in performance are likely to accumulate with ongoing reflections and interference. It is clear from the discrepancies in the response over later periods that, if long-term results are required, more work must be done to improve the accuracy of the off-line pocket model and the overall MOC and SFR equations for the 1D case. Despite the inclusion of 1D unsteady friction, discrepancies accumulate between the modelled outputs and experimental data at later periods as the errors in the prediction accumulate from one period to the next. This is also observed in other studies for similar applications (Bergant et al. 2008). It is recommended that 3D CFD modelling as implemented by Zhou et al. (2018) for the dead-end case be considered as part of future work to better understand the significance of thermal dissipation and friction for this application. Although this approach is more computationally demanding, it may provide additional insight into the governing physical processes.

The findings of this investigation are limited by the range of the experimental conditions tested. Both SFR models do not account for changes in the level of the air-water interface with time due to transient disturbances, suggesting the MOC may be better suited to large transients which result in significant volume changes. The SFR-PW may be well suited to large cavity volumes, such as the surge tank scenario, where travel through the connecting section becomes more important. It is recommended that future investigations explore the effect of transient size and pulse duration, as well as cavity dimensions and assumptions regarding friction within the cavity, to further improve understanding of the modelling approaches available for off-line pockets. It is also recommended that future field investigations aim to better understand and quantify the interference of air pockets in transient assessments of real pipelines. The approach could also be investigated for the surge chamber application.

DATA AVAILABILITY STATEMENT

All data, models, or code that support the findings of this study are available from the corresponding author upon reasonable request.

ACKNOWLEDGMENTS

We would like to thank Hong Kong Research Grants Council for the theme based research scheme (TRS) Grant No. T21-602/15R for supporting this research.

NOTATION

The following symbols are used in this paper:

A = pipe cross-sectional area

a = pipeline wave speed

C_A = polytropic constant

D = pipe diameter

H = pressure head

h = DFT amplitude

h_f = total friction loss

i = spatial index

j = temporal index

k = wavenumber

L = pipe length

L_{cavity} = off-line cavity length

n = polytropic exponent

P = pressure

P_0 = ambient pressure

Q = flow

r = pipe radius

R = reflection coefficient

T = transmission coefficient

t = time

U = velocity

$\forall$ = air pocket volume

W = weighting function

x = distance

z = elevation

ν = kinematic viscosity

ρ = density and

ω = frequency.

REFERENCES

Al-Tofan, M., Elkholy, M., Khilqa, S., Caicedo, J., and Chaudhry, M. H. (2019). "Use of lower harmonics of pressure oscillations for blockage detection in liquid pipelines." *Journal of Hydraulic Engineering*, 145(3), 04018090.

Al-Tofan, M., Elkholy, M., Khilqa, S., and Chaudhry, M. H. (2020). "Leak detection in liquid pipelines using lower harmonics of pressure oscillations." *Journal of Pipeline Systems Engineering and Practice*, 11(4), 04020033.

Alexander, J., Lee, P. J., Davidson, M., Duan, H.-F., Li, Z., Murch, R., Meniconi, S., and Brunone, B. (2019). "Experimental validation of existing numerical models for the interaction of fluid transients with in-line air pockets." *Journal of Fluids Engineering*, 141(12), 121101.

Alexander, J., Lee, P. J., Davidson, M., Li, Z., Murch, R., Duan, H.-F., Meniconi, S., and Brunone, B. (2020a). "Experimental investigation of the interaction of fluid transients with an in-line air pocket." *Journal of Hydraulic Engineering*, 146(3).

Alexander, J., Li, Z., Lee, P. J., Davidson, M., Duan, H.-F., and Murch, R. (2020b). "Experimental investigation of the effects of air pocket configuration on fluid transients in a pipeline (ACCEPTED)." *Journal of Hydraulic Engineering*.

Bergant, A., Simpson, A. R., and Tijsseling, A. S. (2006). "Water hammer with column separation: A historical review." *Journal of Fluids and Structures*, 22(2), 135–171.

Bergant, A., Tijsseling, A. S., Vítkovskỳ, J. P., Covas, D. I., Simpson, A. R., and Lambert, M. F. (2008). "Parameters affecting water-hammer wave attenuation, shape and timing — Part 1: Mathematical tools." *Journal of Hydraulic Research*, 46(3), 373–381.

Burrows, R. and Qiu, D. (1995). "Effect of air pockets on pipeline surge pressure.." *Proceedings of the Institution of Civil Engineers-Water Maritime and Energy*, 112(4), 349–361.

Chaudhry, M. H. (1979). *Applied hydraulic transients*. Springer.

De Martino, G. and Fontana, N. (2012). "Simplified approach for the optimal sizing of throttled air chambers." *Journal of Hydraulic Engineering*, 138(12), 1101–1109.

Duan, H. and Lee, P. (2016). "Transient-based frequency domain method for dead-end side branch detection in reservoir pipeline-valve systems." *Journal of Hydraulic Engineering*, 142(2), 04015042.

Duan, H., Lee, P., Che, T., Ghidaoui, M., Karney, B., and Kolyshkin, A. (2017). "The influence of non-uniform blockages on transient wave behavior and blockage detection in pressurized water pipelines." *Journal of Hydro-environment Research*, 17, 1–7.

Duan, H.-F. (2017). "Transient frequency response based leak detection in water supply pipeline systems with branched and looped junctions." *Journal of Hydroinformatics*, 19(1), 17–30.

Duan, H.-F., Che, T.-C., Lee, P. J., and Ghidaoui, M. S. (2018). "Influence of nonlinear turbulent friction on the system frequency response in transient pipe flow modelling and analysis." *Journal of Hydraulic Research*, 56(4), 451–463.

Duan, H.-F., Lee, P. J., Ghidaoui, M. S., and Tung, Y.-K. (2012). "Extended blockage detection in pipelines by using the system frequency response analysis." *Journal of Water Resources Planning and Management*, 138(1), 55–62.

Evans, W. and Crawford, C. (1954). "Design charts for air chambers on pump lines." *Transactions of the American Society of Civil Engineers*, 119(1), 1025–1036.

Fok, A. T. (1978). "Design charts for air chamber on pump pipe lines." *Journal of the Hydraulics*

Division, 104(9), 1289–1303.

Gong, J., Lambert, M. F., Simpson, A. R., and Zecchin, A. C. (2014). "Detection of localized deterioration distributed along single pipelines by reconstructive MOC analysis." *Journal of Hydraulic Engineering*, 140(2), 190–198.

Graze, H. and Forrest, J. (1974). "New design charts for air chambers." *Fifth Australasian Conference on Hydraulics and Fluid Mechanics*, 34–41.

Jönsson, L. (1985). "Maximum transient pressures in a conduit with check valve and air entrainment." *International Conference on the Hydraulics of Pumping Stations*, 55–76.

Jönsson, L. and Larson, M. (1992). "Leak detection through hydraulic transient analysis." *Pipeline Systems*, Springer, 273–286.

Karney, B. W. and McInnis, D. (1992). "Efficient calculation of transient flow in simple pipe networks." *Journal of Hydraulic Engineering*, 118(7), 1014–1030.

Kim, S. H. (2008a). "Impulse response method for pipeline systems equipped with water hammer protection devices." *Journal of Hydraulic Engineering*, 134(7), 961–969.

Kim, Y. I. (2008b). "Advanced numerical and experimental transient modelling of water and gas pipeline flows incorporating distributed and local effects." Ph.D. thesis, University of Adelaide, Adelaide, Australia.

Kinsler, L. E., Frey, A. R., Coppens, A. B., and Sanders, J. V. (2000). *Fundamentals of Acoustics*. John Wiley & Sons Inc, New York.

Lauchlan, C., Escarameia, M., May, R., Burrows, R., and Gahan, C. (2005). "Air in pipelines: A literature review." Vol. 649, HR Wallingford. Report SR, Oxford, United Kingdom.

Lee, N. and Martin, C. (1999). "Experimental and analytical investigation of entrapped air in a horizontal pipe." *Proceedings of the 3rd ASME/JSME Joint Fluids Engineering Conference, San Francisco USA, July 18-23*, 189–196.

Lee, N. H. (2005). "Effect of pressurization and expulsion of entrapped air in pipelines." Ph.D. thesis, Georgia Institute of Technology, Atlanta, USA.

Lee, P. J., Duan, H.-F., Ghidaoui, M., and Karney, B. (2013). "Frequency domain analysis of pipe

fluid transient behaviour." *Journal of Hydraulic Research*, 51(6), 609–622.

Lee, P. J., Vítkovskỳ, J. P., Lambert, M. F., Simpson, A. R., and Liggett, J. A. (2005). "Frequency domain analysis for detecting pipeline leaks." *Journal of Hydraulic Engineering*, 131(7), 596–604.

Lee, P. J., Vítkovskỳ, J. P., Lambert, M. F., Simpson, A. R., and Liggett, J. A. (2008). "Discrete blockage detection in pipelines using the frequency response diagram: Numerical study." *Journal of Hydraulic Engineering*, 134(5), 658–663.

Martin, C. and Wiggert, D. (1986). "Hydraulic transients in circulating cooling water systems." *Report no.*, Electric Power Research Institute, Georgia Inst. of Technology and Michigan State University.

Martin, F. (2015). *Artificial transmission lines for RF and microwave applications*. John Wiley & Sons.

Orfanidis, S. J. (2002). *Electromagnetic waves and antennas*. Rutgers University New Brunswick, NJ.

Purcell, P. J. (1997). "Case study of check-valve slam in rising main protected by air vessel." *Journal of Hydraulic Engineering*, 123(12), 1166–1168.

Stephens, M., Lambert, M., Simpson, A., Vítkovskỳ, J., and Nixon, J. (2004a). "Field tests for leakage, air pocket, and discrete blockage detection using inverse transient analysis in water distribution pipes." *Critical Transitions in Water and Environmental Resources Management*, 1–10.

Stephens, M., Vitkovsky, J., Lambert, M., Simpson, A., Karney, B., and Nixon, J. (2004b). "Transient analysis to assess valve status and topology in pipe networks." *9th International Conference on Pressure Surges*.

Vasconcelos, J. G. and Leite, G. M. (2012). "Pressure surges following sudden air pocket entrapment in storm-water tunnels." *Journal of Hydraulic Engineering*, 138(12), 1081–1089.

Vítkovskỳ, J., Lambert, M., Simpson, A., and Bergant, A. (2003). "Frequency-domain transient pipe flow solution including unsteady friction." *Proceedings of the International Conference on*

560 *Pumps, Electromechanical Devices and Systems Applied to Urban Water Management*, 773–780.
561 Wood, D. J., Lingireddy, S., Boulos, P. F., Karney, B. W., and McPherson, D. L. (2005). "Numerical
562 methods for modeling transient flow in distribution systems." *Journal-American Water Works*
563 *Association*, 97(7), 104–115.
564 Wylie, E. B., Streeter, V. L., and Suo, L. (1993). *Fluid transients in systems*, Vol. 1. Prentice Hall
565 Englewood Cliffs, NJ.
566 Xu, X. and Karney, B. (2017). "An overview of transient fault detection techniques." *Modeling and*
567 *monitoring of pipelines and networks*, Springer, 13–37.
568 Zhou, F. (2000). "Effects of trapped air on flow transients in rapidly filling sewers." Ph.D. thesis,
569 University of Alberta, Edmonton, Canada.
570 Zhou, L., Liu, D., Karney, B., and Wang, P. (2013). "Phenomenon of white mist in pipelines rapidly
571 filling with water with entrapped air pockets." *Journal of Hydraulic Engineering*, 139(10),
572 1041–1051.
573 Zhou, L., Liu, D., Karney, B., and Zhang, Q. (2011). "Influence of entrapped air pockets on hydraulic
574 transients in water pipelines." *Journal of Hydraulic Engineering*, 137(12), 1686–1692.
575 Zhou, L., Wang, H., Karney, B., Liu, D., Wang, P., and Guo, S. (2018). "Dynamic behavior of
576 entrapped air pocket in a water filling pipeline." *Journal of Hydraulic Engineering*, 144(8),
577 04018045.
578 Zielke, W. (1968). "Frequency-dependent friction in transient pipe flow." *Journal of Basic Engi-*
579 *neering*, 90(1), 109–115.

List of Figures

Fig. 1. Diagram of experimental set-up. Section A-A' is shown in Fig. 2.

Fig. 2. Section A-A': Diagram of crest section and off-line cavity

Fig. 3. Schematic for off-line cavity governing MOC equations

Fig. 4. Schematic for off-line cavity governing transfer matrix equations

Fig. 5. Experimental and modelled transient pressure traces at PT2, upstream of the pocket, for an off-line air pocket at 2.0 bar for (a) L_a^*=0.20, (b) L_a^*=0.51, and (c) L_a^*=0.84.

Fig. 6. Experimental and modelled transient pressure traces at PT3, downstream of the pocket, for an off-line air pocket at 2.0 bar for (a) L_a^*=0.20, (b) L_a^*=0.51, and (c) L_a^*=0.84.

Fig. 7. Time delay between the incident peak arrival time and the (a) reflected peak arrival time at PT2 and (b) transmitted peak arrival time at PT3.

Fig. 8. Experimental and modelled DFT amplitudes for an off-line air pocket at 2.0 bar, L_a^*=0.51, for (a) the first reflected pulse, and (b) the first transmitted pulse.

Fig. 9. Root mean squared error for the MOC, SFR-LI, and SFR-PW models for compared to experimental observations for (a) the first reflected pulse DFT, and (b) the first transmitted pulse DFT.

Figure 1

Click here to access/download;Figure;Fig1.eps

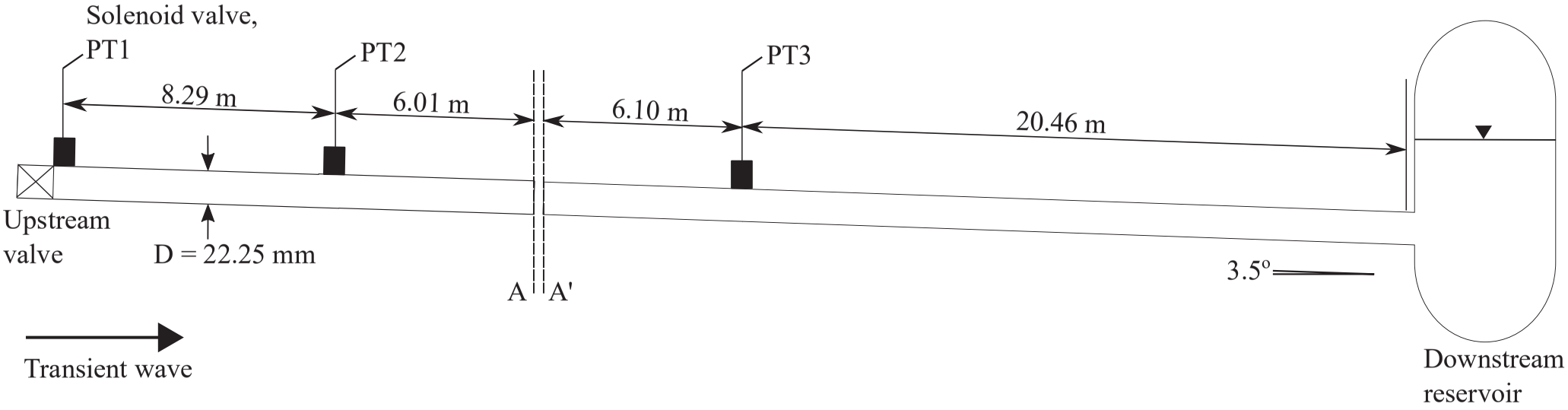

Figure 2

Click here to access/download;Figure;Fig2.eps

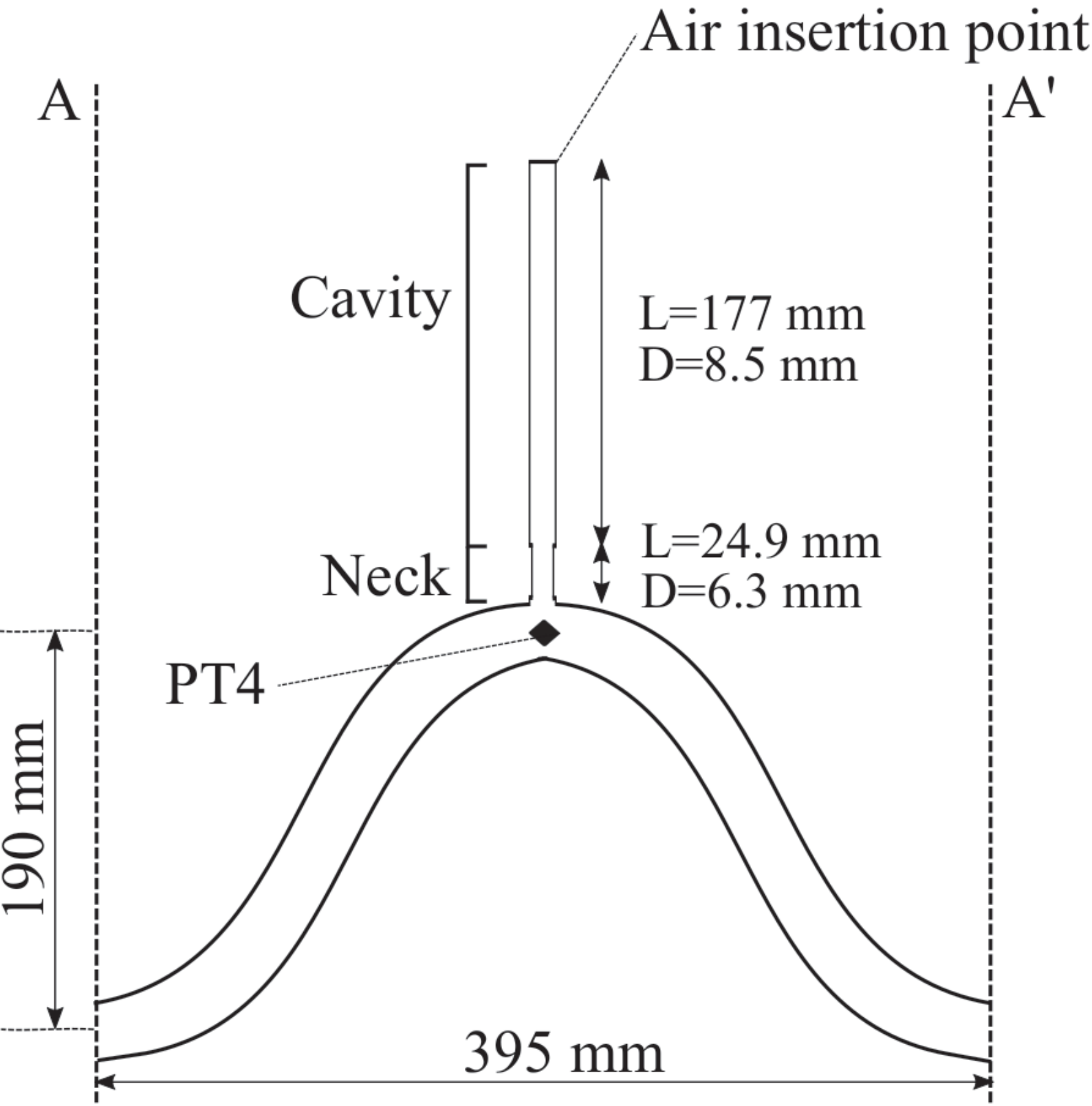

Figure 1

Click here to access/download;Figure;Fig3.eps

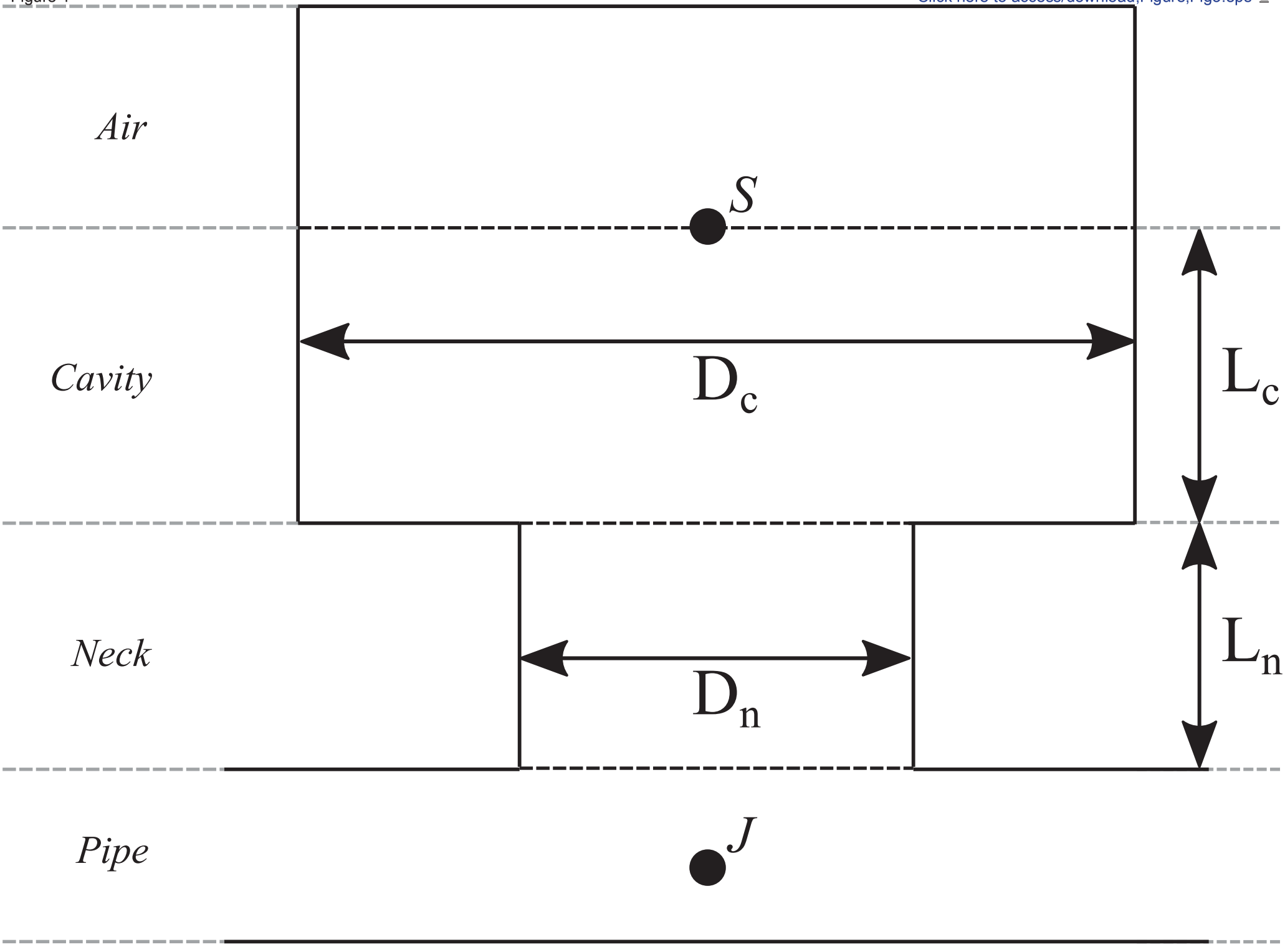

Figure 4

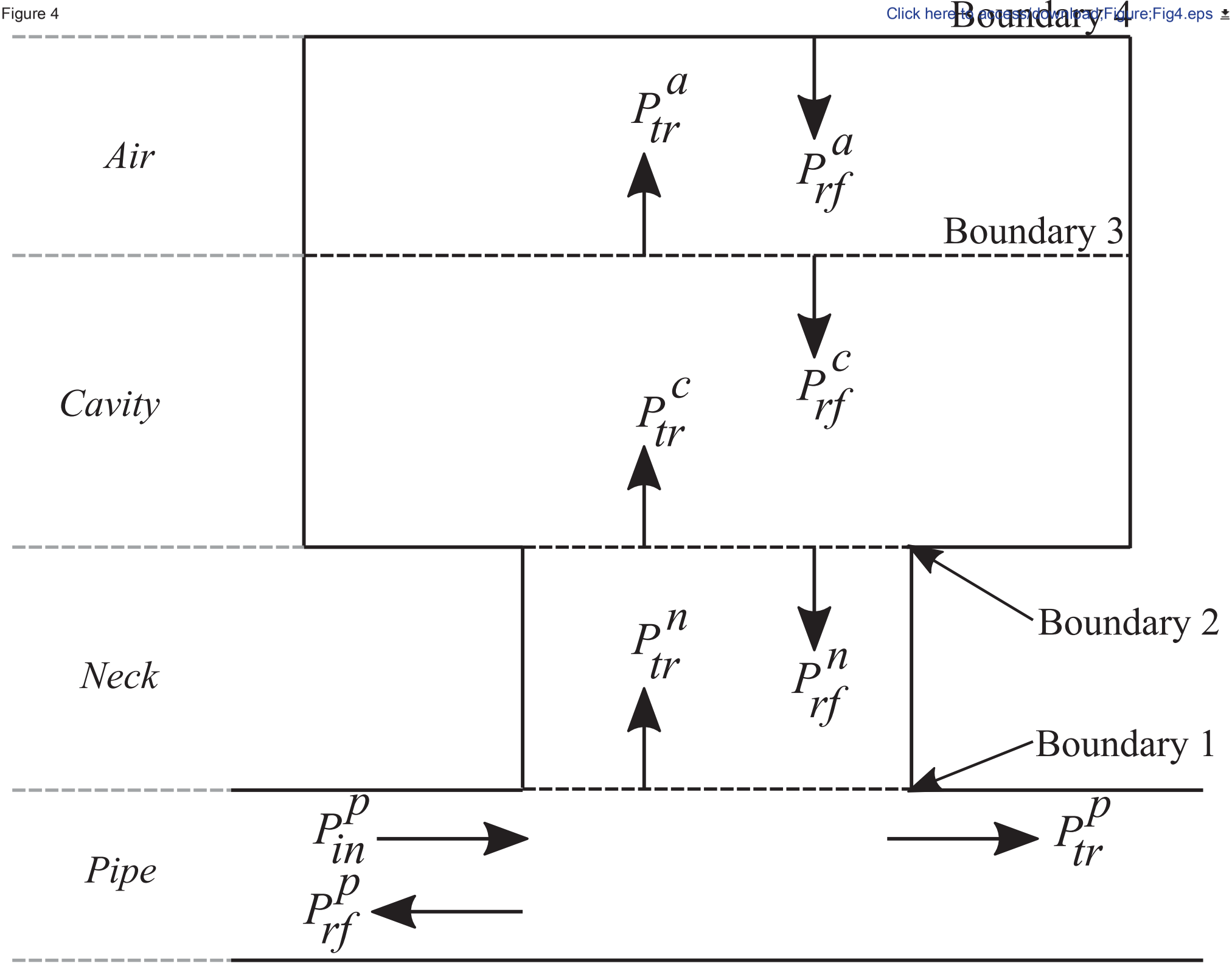

Figure 5

Click here to access/download;Figure;Fig5.eps

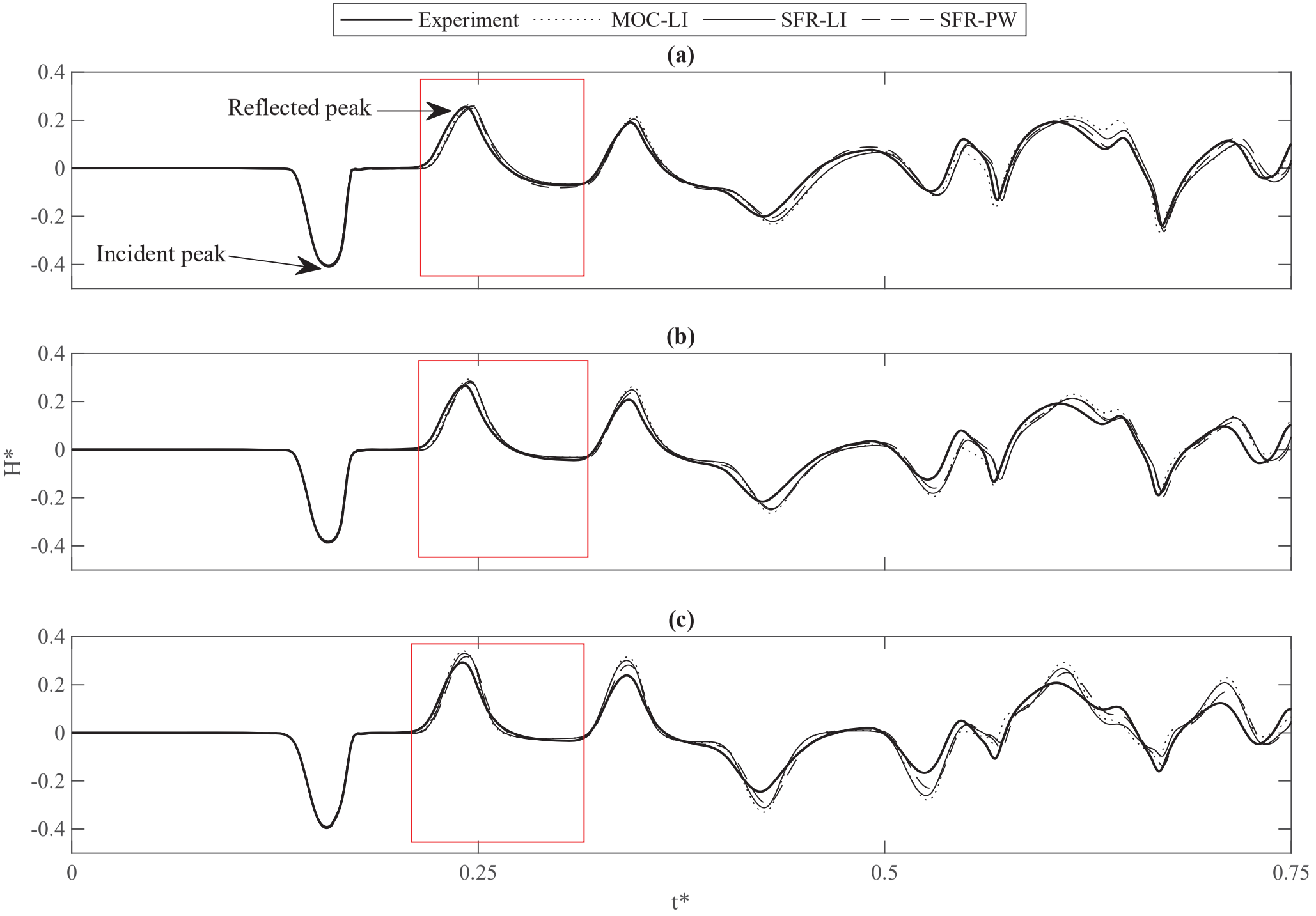

Figure 6

Click here to access/download;Figure;Fig6.eps

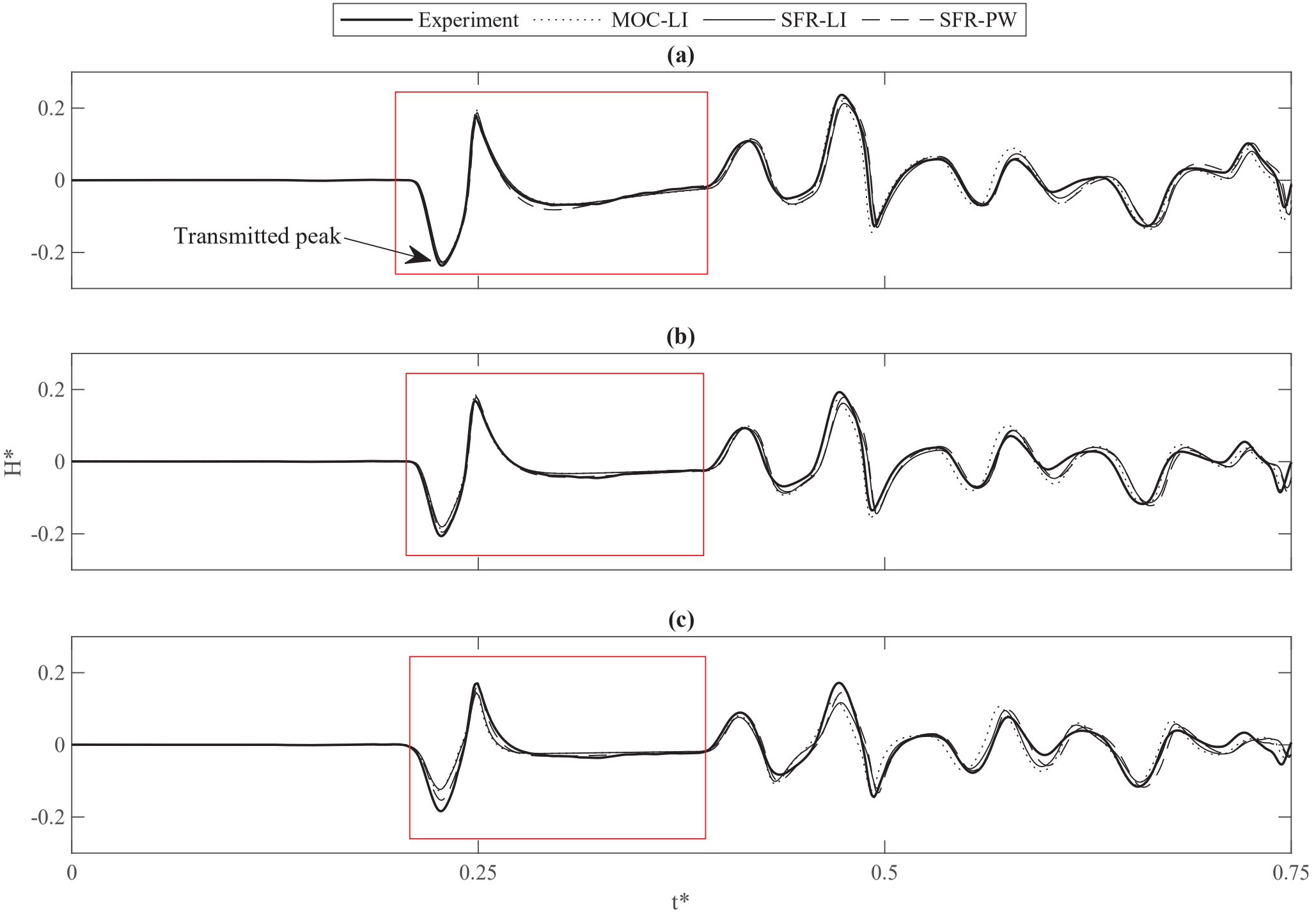

Figure 7

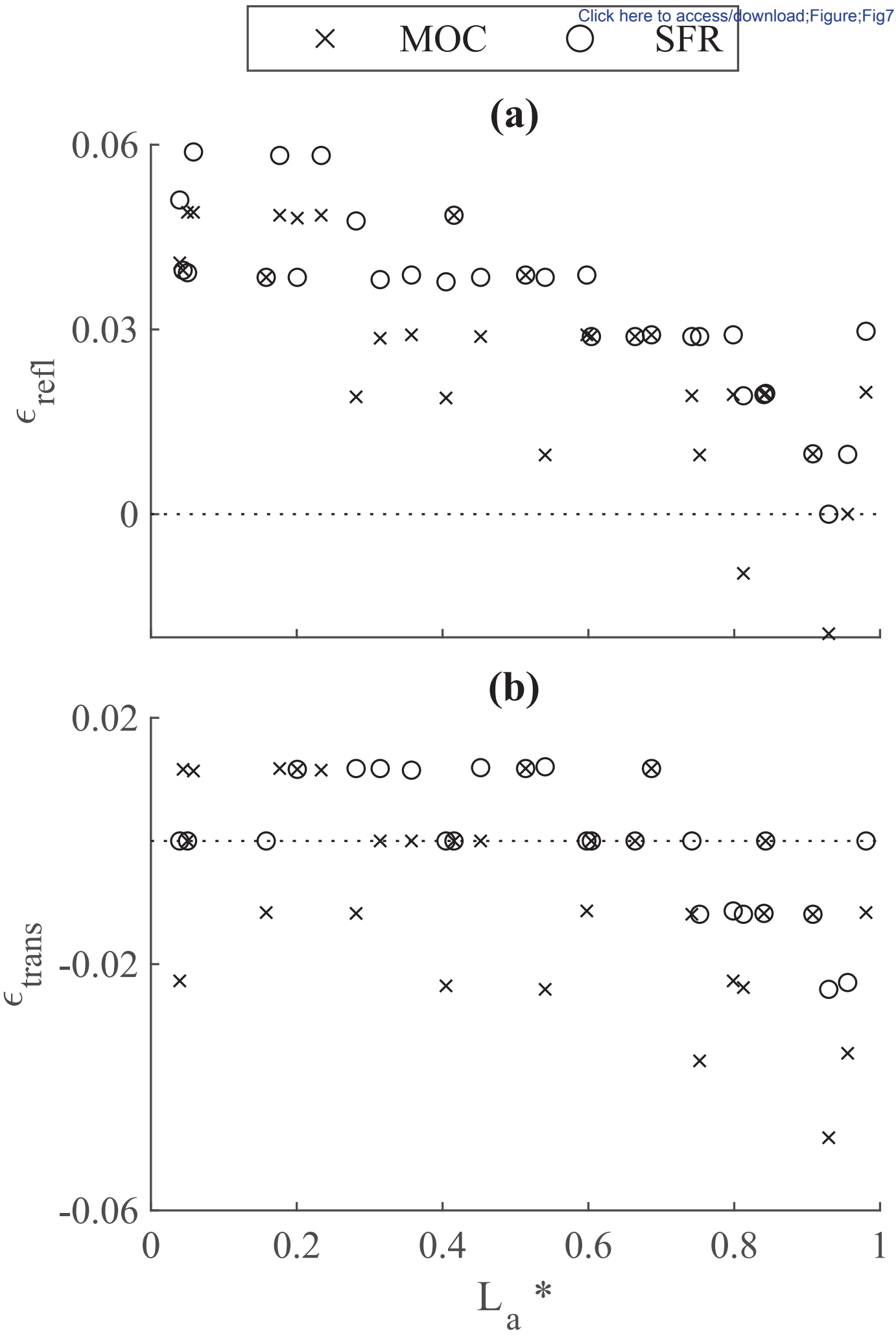

Figure 8

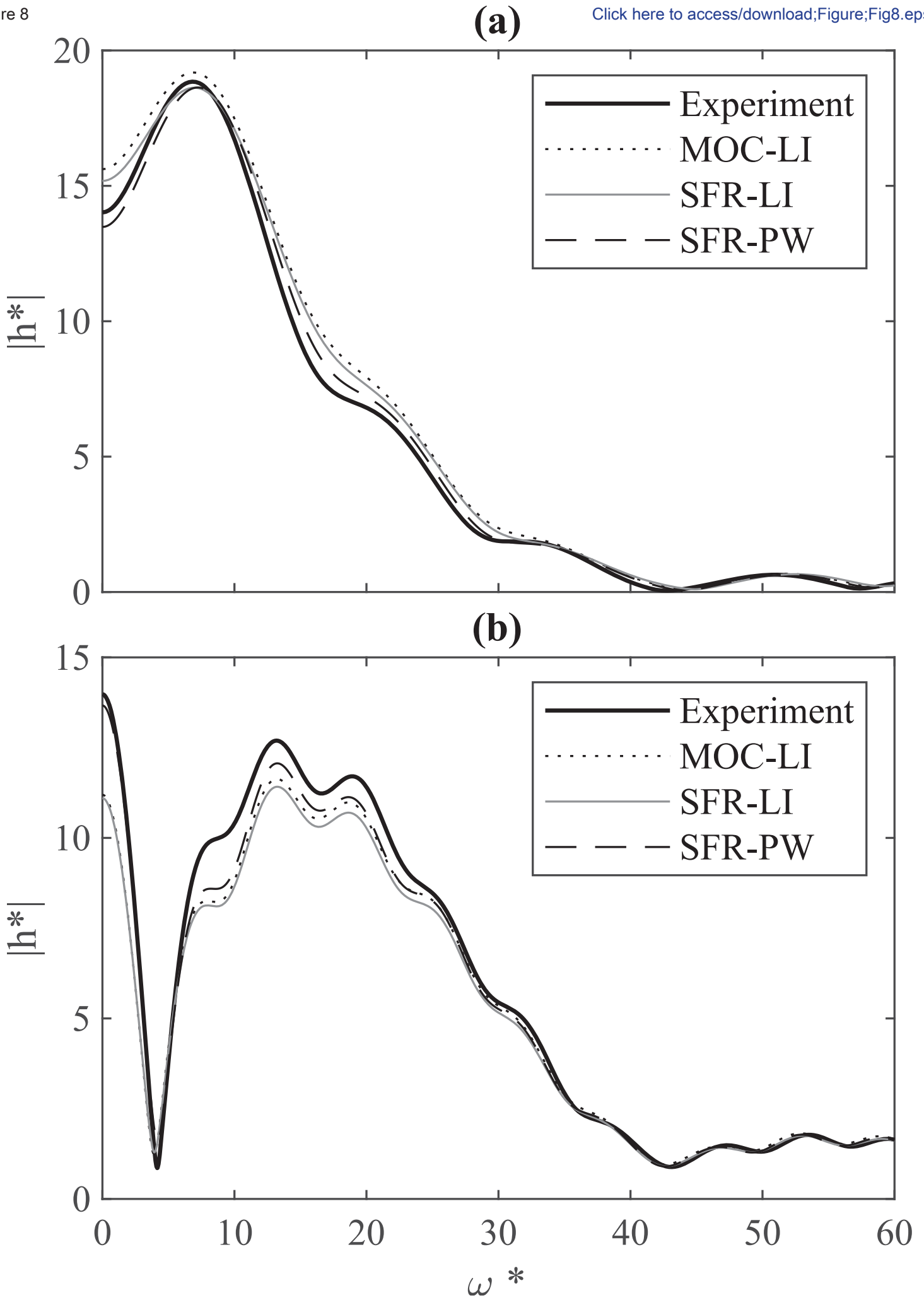

Figure 9